Optimal path planning for fixed-wing UAVs in 3D space

Conference Paper · February 2018

CITATIONS
0

READS
469

2 authors:

Nikhil Kumar Singh
Indian Institute of Technology Kharagpur
5 PUBLICATIONS **4** CITATIONS
SEE PROFILE

Sikha Hota
Indian Institute of Science
14 PUBLICATIONS **114** CITATIONS
SEE PROFILE

Proceedings of ICTACEM 2017
International Conference on Theoretical, Applied, Computational and Experimental Mechanics
December 28-30, 2017, IIT Kharagpur, India
ICTACEM-2017/654

Optimal path planning for fixed-wing UAVs in 3D space

Nikhil Kumar Singh[a] and Sikha Hota[b*]

[a] Research Scholar, Department of Aerospace Engineering, IIT Kharagpur, Kharagpur 721302, West Bengal, India
[b] Assistant Professor, Department of Aerospace Engineering, IIT Kharagpur, Kharagpur 721302, West Bengal, India

ABSTRACT

This paper presents the optimal path generation algorithm for fixed-wing unmanned aerial vehicles (UAVs) in three-dimensional space (3D) when the initial and final positions and orientations of the vehicle are specified. The problem is very much relevant in the context of waypoint following problem where the UAVs are required to fly through the number of waypoints specified by the given mission. The generated path considers the limit on the turn radius of the vehicle, which arises from the kinematic constraints of the fixed-wing UAVs. It is assumed that the vehicle is flying at a constant airspeed throughout the mission. As the values of minimum turn radiuses are different in different 2D planes of the 3D space, path generation is more challenging compared to existing works in literature. The method presented here is based on 3D geometry and path is of CSC (Circular arc of minimum turn radius of the initial maneuver plane-Straight line-Circular arc of minimum turn radius of the final maneuver plane) types for sufficiently large distances between initial and final positions. The computational time of the proposed approach is considerably low, which makes it implementable in real time.

Keywords: Geometrical method for UAVs, CSC path in 3D space, Optimal path planning of UAVs

1. INTRODUCTION

Recently, unmanned aerial vehicles (UAVs) are used in several dull, dirty and dangerous applications such as, surveillance, battle filled deployment, search and rescue etc. For almost all these missions, optimal path planning is an important problem to consider as it saves the time and fuel consumption of UAVs. The shortest path between given initial and final positions and orientations for a turn-rate constraint vehicle was first developed by Dubins[1] in 2D plane. These paths are of type CCC, CSC or any subset of these, such as CS, SC, CC and so on, where C represents the circular arc of minimum turn radius and S represents a straight line segment. Shkel and Lumelsky[2] proposed different set of Dubins path for large and small distances between initial and final position and orientations. Dubins path is discontinuous when the transition occurs between arc and line segment, so Shanmugavel et al.[3] proposed a quintic Pythagorian hodograph curves in 2D plane which makes the Dubins path continuous. Babaei and Mortazavi[4] proposed an efficient algorithm for fast trajectory planning of unmanned aerial vehicles (UAVs) in 2D plane without the prior knowledge of midcourse waypoints. These

* Further author information: (Send correspondence to N.K.S)
S.H.: E-mail: sikhahota@aero.iitkgp.ernet.in
N.K.S.: E-mail: nikhil.singh@iitkgp.ac.in, Address: Department of Aerospace Engineering, Indian Institute of Technology Kharagpur, Kharagpur 721302, West Bengal, India

midcourse waypoints are computed during online flight using optimal control and geometric principles. In the presence of wind, optimal path planning of miniature air vehicles (MAVs) are challenging, because the wind speed is about 20-60% of the air speed of MAVs. Hota and Ghose[5] presented an optimal straight line path planning for MAVs in 2D plane with wind or without wind environment. Nelson et al.[6] proposed a vector field method for path following of straight line and circular arcs by MAVs in the presence of constant wind but it is not optimal. Park et al.[7] proposed a nonlinear path following guidance method of UAVs for tracking the straight line and curved paths accurately in the presence of wind. Hota and Ghose[8] presented the method in 2D plane for tracking the waypoints as well as entire waypoint segments in time-optimal fashion for MAVs in the presence of wind.

Later, Sussmann[9] discussed the shortest path in 3D space which is either a helicoidal arc or CSC or CCC type path for given initial and final positions and orientations. It also commented that for sufficiently large distance between two points, CSC path is optimal and for small distance, helicoidal path is optimal. But how to compute this CSC path was a difficult issue and which was addressed by Hota and Ghose[10]. This path has a potential applicability in the path planning of fixed-wing UAVs with bounded turn radius flying in 3D space. Pharpatara et al.[11] discussed the 3D shortest path planning for a hypersonic glider in a heterogeneous environment. Cicibas et al.[12] presented the comparison of 3D versus 4D (three spatial dimension and time dimension) path planning of unmanned aerial vehicles and shown that the result of 4D path planning is better than 3D in complex dynamic environment. In another interesting work, Hota and Ghose[13] presented waypoint-based trajectory planning of fixed-wing MAVs in 3D space, where transition between one waypoint segments to another is executed in a smooth manner, without colliding with the obstacles and satisfying the objective of passing through a desired distance from the associated waypoint as well. Pharpatara et al.[14] proposed an obstacle avoidance trajectory planning of an aerial vehicles in 3D space using rapidly exploring random tree (RRT*) algorithm. For increasing the convergence speed of suboptimal solution of RRT* algorithm, it is combined with artificial potential fields.

In this present work, the objective is to optimize the path length between the initial position (X_0) with given orientation ($\boldsymbol{v}_1$) to the final position (X_f) with given orientation ($\boldsymbol{v}_2$) in 3D space. The initial and final points are assumed to be situated sufficiently far away. The problem definition is similar to the one discussed by Hota and Ghose[10]. But in paper[10], for both the circular turns (initial and final), the same turning radius was assumed, which gives a longer path length compared to the path generated in this current work. This is due to the fact that in

paper[10], the minimum turn radius was considered to be the same for all maneuvering planes for simplicity and for that the maximum value of minimum turn radius of all 2D circular maneuvers was considered. In reality, the minimum turn radius (r) of the vehicle depends on the inclination angle (ψ) of the 2D maneuver plane in 3D space. For example, the minimum turn radius in a plane which is parallel to XY plane is less than that of a plane parallel to XZ plane. More specifically, the lowest value of minimum turn radius (r_h) can be achieved if the maneuver is parallel to XY plane and the highest value of minimum turn radius (r_v) is achieved in case of maneuvering parallel to XZ plane. For any other inclined plane the value of minimum turn radius is between these bounds, $r_h \leq r \leq r_v$. From the above discussion it is clear that if the two circular turns (initial and final circular maneuvers of a CSC path) are with different value of turn radiuses ($\leq r_v$), total path length can be made smaller compared to paper[10]. So in this current work, the minimum turn radiuses for both initial and final maneuver planes are different (r_1 and r_2) (see Figure 1) and which can be obtained along with the common tangent between two circular maneuvers by solving a couple of nonlinear equations. The symbols used are tabulated in Table 1, where the bold font represents the notation of vector.

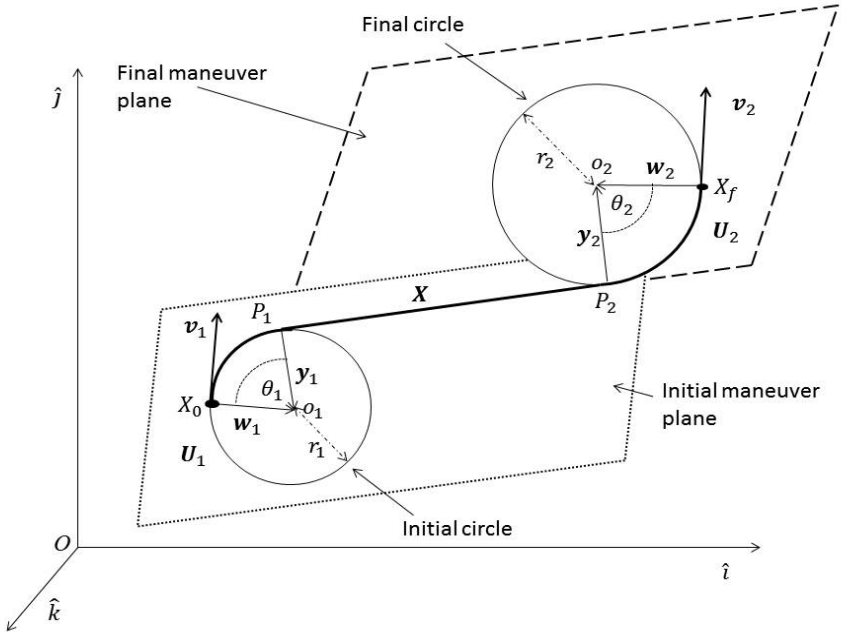

Figure 1: Geometry of CSC path in 3D space for given initial and final positions and orientations.

Table 1: Notations

Symbols	Magnitude of vector	Meaning
X_0		Initial position of the vehicle
X_f		Final position of the vehicle

$\boldsymbol{v}_1$	1		Initial orientation (unit velocity vector) of the vehicle
$\boldsymbol{v}_2$	1		Final orientation (unit velocity vector) of the vehicle
v_a			Airspeed of the aerial vehicle
η			Maximum load factor
ψ			Inclination angle of the 2D maneuver plane with X-Y plane
r			Minimum turn radius in an inclined plane
r_h			Minimum turn radius in horizontal plane
r_v			Minimum turn radius in vertical plane
$\boldsymbol{L}$	L		Lift force
$\boldsymbol{W}$	W		Weight of the UAV
$\boldsymbol{F}_r$	F_r		Radial force
m			Mass of the UAV
ϕ			Banking angle
$\boldsymbol{g}$	g		Acceleration due to gravity
$\boldsymbol{X}$	X		Tangent vector between initial and final maneuver circle
$\boldsymbol{x}$	1		Unit tangent vector along $\boldsymbol{X}$
P_1			Intersection point between initial maneuver circle and $\boldsymbol{X}$
P_2			Intersection point between final maneuver circle and $\boldsymbol{X}$
$\boldsymbol{U}_1$		U_1	Normal vector on initial maneuver plane
$\boldsymbol{U}_2$		U_2	Normal vector on final maneuver plane
$\boldsymbol{u}_1$	1		Unit normal vector on initial maneuver plane
$\boldsymbol{u}_2$	1		Unit normal vector on final maneuver plane
O			Origin of the coordinate system
O_1			Origin of the initial maneuver circle
O_2			Origin of the final maneuver circle
ψ_1			Angle between initial maneuver plane and X-Y plane
ψ_2			Angle between final maneuver plane and X-Y plane
r_1			Minimum turn radius of the initial maneuver circle
r_2			Minimum turn radius of the final maneuver circle
θ_1			Initial angular turn
θ_2			Final angular turn
$\boldsymbol{W}_1$		W_1	Radius vector pointing from X_0 to O_1
$\boldsymbol{W}_2$	W_2		Radius vector pointing from X_f to O_2
$\boldsymbol{w}_1$	1		Unit radius vector pointing from X_0 to O_1
$\boldsymbol{w}_2$	1		Unit radius vector pointing from X_f to O_2
$\boldsymbol{Y}_1$	Y_1		Radius vector pointing from P_1 to O_1
$\boldsymbol{Y}_2$	Y_2		Radius vector pointing from P_2 to O_2
$\boldsymbol{y}_1$	1		Unit radius vector pointing from P_1 to O_1
$\boldsymbol{y}_2$	1		Unit radius vector pointing from P_2 to O_2

2. PROBLEM FORMULATION

Path planning of fixed-wing UAVs is considered in 3D space, where airspeed (v_a) and maximum load factor (η) of the vehicle are assumed to be constant throughout the mission. The UAV has different values of minimum turn radiuses different inclined planes. The front view of the UAV is shown in Figure 2, where the UAV's plane of maneuver makes the angle ψ with the horizontal plane (X-Y plane). The wings of the UAVs are banked at an angle ϕ to facilitate a turn on the tilted plane. From the force-balance equations of the UAV we get,

$$W \cos\psi = L \cos(\psi + \phi) \tag{1}$$

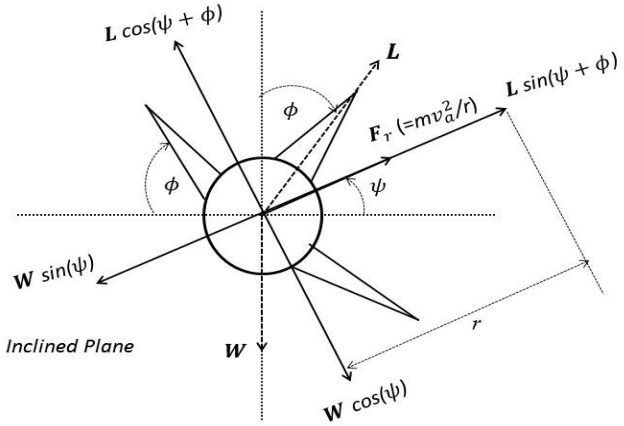

Figure 2: Geometry for computing the minimum turn radius in inclined plane.

Radial force $\boldsymbol{F}_r$ is defined as,

$$F_r = \frac{mv_a^2}{r} = L \sin(\psi + \phi) - W \sin\psi \tag{2}$$

By replacing $\eta = L/W$ in equations (1) and (2), we get the turn radius of the inclined plane as,

$$r = \frac{v_a^2}{g(-\sin\psi + \sqrt{\eta^2 + sin^2\psi - 1})} \tag{3}$$

For all planes, minimum radius of circular turn can occur only when the value of load factor is maximum.

In equation (3), if $\psi = 0$ (the plane corresponds to the horizontal plane or X-Y plane), we get turn radius r_h as,

$$r_h = \frac{v_a^2}{g\sqrt{\eta^2-1}} \quad (4)$$

And if, $\psi = \frac{\pi}{2}$ (the plane corresponds to the vertical plane or X-Z plane), we get turn radius r_v as,

$$r_v = \frac{v^2}{g(\eta-1)} \quad (5)$$

Note that, the value of minimum turn radius on the vertical plane is more compared to the same on the horizontal plane, or, $r_v > r_h$.

3. 3D PATH GENERATION

The geometrical method generates the optimal path of CSC type when initial and final points are situated sufficiently far away. The principle of the path generation is the same as of 2D plane but the values of minimum turn radiuses are different in different maneuver planes. The 2D plane on which the initial maneuver will take place will be called as the initial maneuvering plane and similarly, the 2D plane on which the final maneuver will take place will be called as the final maneuvering plane. Note that, the straight line maneuver between these two turns is along the straight line which is the common tangent between these two circular turns and is also the intersecting line between the initial and final maneuvering planes. A typical CSC path in 3D space is shown in Figure 1. As mentioned earlier, the values of minimum turn radiuses for the initial and final maneuvering planes are different and they are denoted as r_1 and r_2, respectively. To compute the CSC path, the following steps will be followed.

Let us define, $\boldsymbol{X}$ be the tangent vector between the two circular maneuvers as shown in Fig. 1. The unit vector along $\boldsymbol{X}$ is,

$$\boldsymbol{x} = \frac{\boldsymbol{X}}{X} \quad (6)$$

The vector perpendicular to the initial maneuver plane is defined as,

$$\boldsymbol{U}_1 = \boldsymbol{x} \times \boldsymbol{v}_1 \quad (7)$$

Where the unit normal vector to initial maneuver plane is, $\boldsymbol{u}_1 = \frac{\boldsymbol{U_1}}{U_1}$. The minimum turn radius corresponds to the initial maneuver plane will be,

$$r_1 = \frac{v_a^2}{g(-\sin\psi_1+\sqrt{\eta^2+sin^2\psi_1-1})}. \quad (8)$$

Where $\psi_1 = cos^{-1}(\boldsymbol{u}_1.(0,0,1))$. The radius vector $\boldsymbol{W}_1$, which is oriented toward the center of the initial circle from its initial position is,

$$\boldsymbol{W}_1 = \boldsymbol{v}_1 \times \boldsymbol{U}_1 = \boldsymbol{v}_1 \times (\boldsymbol{x} \times \boldsymbol{v}_1) \quad (9)$$

The position vector of the center of the initial circle $\boldsymbol{OO}_1$ can be written as,

$$\boldsymbol{OO}_1 = \boldsymbol{OX}_0 + r_1\boldsymbol{w}_1 \quad (10)$$

Where $\boldsymbol{w}_1 = \frac{\boldsymbol{W}_1}{W_1}$. Then, the radius vector $\boldsymbol{Y}_1$, which is oriented towards the center of the initial circle from the point P_1 where the aerial vehicle starts following the straight line path and tangential to both initial and final maneuver circles, is

$$\boldsymbol{Y}_1 = \boldsymbol{x} \times \boldsymbol{U}_1 = \boldsymbol{x} \times (\boldsymbol{x} \times \boldsymbol{v}_1) \tag{11}$$

The point P_1 where the straight line touch the initial circle is defined as,

$$\boldsymbol{OP}_1 = \boldsymbol{OO}_1 - r_1\boldsymbol{y}_1 = \boldsymbol{OX}_0 + r_1\boldsymbol{w}_1 - r_1\boldsymbol{y}_1 \tag{12}$$

Where $\boldsymbol{y}_1 = \frac{\boldsymbol{Y}_1}{Y_1}$. The vector perpendicular to the final maneuver plane is defined as,

$$\boldsymbol{U}_2 = \boldsymbol{x} \times \boldsymbol{v}_2 \tag{13}$$

Where the unit normal vector to final maneuver plane is $\boldsymbol{u}_2 = \frac{\boldsymbol{U}_2}{U_2}$. The minimum turn radius of the final maneuver circle is calculated as,

$$r_2 = \frac{v_a^2}{g(-\sin\psi_2 + \sqrt{\eta^2 + sin^2\psi_2 - 1})} \tag{14}$$

Where $\psi_2 = cos^{-1}(\boldsymbol{u}_2.(0,0,1))$. The radius vector $\boldsymbol{W}_2$ which is oriented toward the center of the final circle from its final position is defined as,

$$\boldsymbol{W}_2 = -\boldsymbol{v}_2 \times \boldsymbol{U}_2 = -\boldsymbol{v}_2 \times (\boldsymbol{x} \times \boldsymbol{v}_2) \tag{15}$$

The center position vector of the final circle $\boldsymbol{OO}_2$ is defined as,

$$\boldsymbol{OO}_2 = \boldsymbol{OX}_f + r_2\boldsymbol{w}_2 \tag{16}$$

Where, $\boldsymbol{w}_2 = \frac{\boldsymbol{W}_2}{W_2}$. Then, the radius vector $\boldsymbol{Y}_2$, which is oriented towards the center of the final circle from the point P_2 where the aerial vehicle starts following the circular curve to the final circle, is defined as,

$$\boldsymbol{Y}_2 = -\boldsymbol{x} \times \boldsymbol{U}_2 = -\boldsymbol{x} \times (\boldsymbol{x} \times \boldsymbol{v}_2) \tag{17}$$

The point P_2 where the straight line touches the final circle is defined as,

$$\boldsymbol{OP}_2 = \boldsymbol{OO}_2 - r_2\boldsymbol{y}_2 = \boldsymbol{OX}_f + r_2\boldsymbol{w}_2 - r_2\boldsymbol{y}_2 \tag{18}$$

Where, $\boldsymbol{y}_2 = \frac{\boldsymbol{Y}_2}{Y_2}$, Now, we can find the value of $\boldsymbol{X}$ by solving the following nonlinear equation as,

$$\boldsymbol{OP}_2 - \boldsymbol{OP}_1 = \boldsymbol{X} = \left(\boldsymbol{OX}_f + r_2\boldsymbol{w}_2 - r_2\boldsymbol{y}_2\right) - (\boldsymbol{OX}_0 + r_1\boldsymbol{w}_1 - r_1\boldsymbol{y}_1) \tag{19}$$

$$\boldsymbol{OP}_2 - \boldsymbol{OP}_1 = \boldsymbol{X} = \boldsymbol{OX}_f - \boldsymbol{OX}_0 - r_1(\boldsymbol{w}_1 - \boldsymbol{y}_1) - r_2(\boldsymbol{y}_2 - \boldsymbol{w}_2) \tag{20}$$

From Figure 3(a) we get,

$$r_1(\boldsymbol{w}_1 - \boldsymbol{y}_1) = \boldsymbol{X}_0\boldsymbol{P}_1 = \boldsymbol{X}_0\boldsymbol{Q} + \boldsymbol{QP}_1 = r_1\tan\left(\frac{\theta_1}{2}\right)\boldsymbol{v}_1 + r_1\tan\left(\frac{\theta_1}{2}\right)\boldsymbol{x} \tag{21}$$

From Figure 3(b) we get,

$$r_2(\boldsymbol{y}_2 - \boldsymbol{w}_2) = \boldsymbol{P}_2\boldsymbol{X}_f = \boldsymbol{P}_2\boldsymbol{R} + \boldsymbol{R}\boldsymbol{X}_f = r_2\tan\left(\frac{\theta_2}{2}\right)\boldsymbol{x} + r_2\tan\left(\frac{\theta_2}{2}\right)\boldsymbol{v}_2 \tag{22}$$

Here, θ_1 and θ_2 follow the following relationships: $cos\,\theta_1 = \boldsymbol{v}_1.\boldsymbol{x}$ and $cos\,\theta_2 = \boldsymbol{v}_2.\boldsymbol{x}$.
Using (21) and (22) the equation (20) can be written as,

$$\boldsymbol{X} = \boldsymbol{OX}_f - \boldsymbol{OX}_0 - r_1 \tan\left(\frac{\theta_1}{2}\right)(\boldsymbol{x} + \boldsymbol{v}_1) - r_2 \tan\left(\frac{\theta_2}{2}\right)(\boldsymbol{x} + \boldsymbol{v}_2) \quad (23)$$

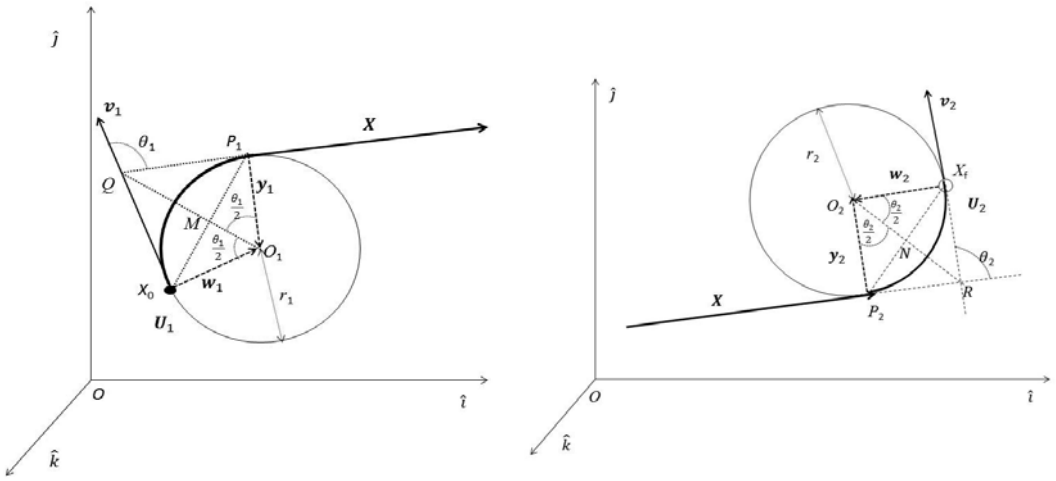

(a) **(b)**

Figure 3: (a) The initial maneuver turn in 3D space **(b)** The final maneuver turn in 3D space.

Solving these nonlinear equations, we can obtain$\boldsymbol{X}$, θ_1, θ_2 , r_1 and r_2. Now, the total length of the path can be computed as,

The total length of the CSC path = first arc length ($r_1\theta_1$) + straight line length (X) + second arc length ($r_2\theta_2$)).

It is important to note that there can be four types of CSC paths for this problem. The complete set of equations is,

$$\boldsymbol{X} = \boldsymbol{OX}_f - \boldsymbol{OX}_0 \mp r_1 \tan\left(\frac{\theta_1}{2}\right)(\boldsymbol{x} + \boldsymbol{v}_1) \mp r_2 \tan\left(\frac{\theta_2}{2}\right)(\boldsymbol{x} + \boldsymbol{v}_2) \quad (24)$$

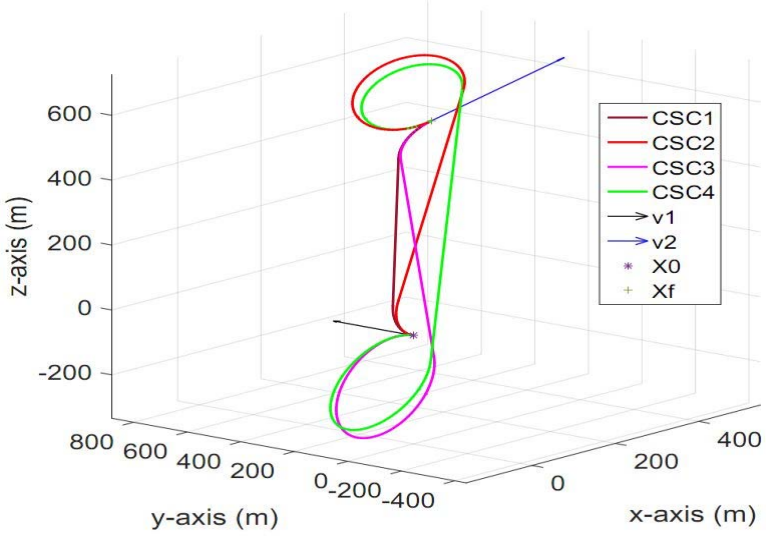

Figure 4: Four CSC paths in 3D space.

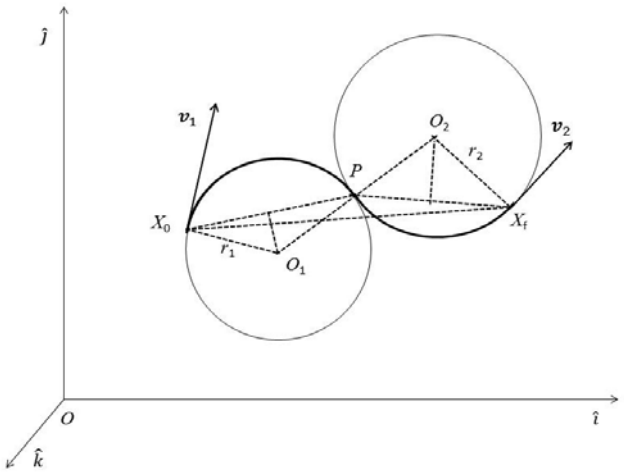

Figure 5: Sufficient distance between initial and final points to obtain CSC path.

Example: In Figure 4, the four CSC paths are shown for given initial and final conditions. Here X_0 = (0, 0, 0), $\boldsymbol{v}_1$ = (0, 1, 0), X_f = (300, 400, 500), and $\boldsymbol{v}_2$ = (0.8270, -0.3678, 0.4252). The other values of parameters are shown in Table 2. The lengths of the CSC paths are as follows: CSC1= 742.1491 m, CSC2= 1277.2 m, CSC3= 1367.9 m, CSC4 = 1840.7 m.

Table 2: Simulation parameters

Parameters	Value
Airspeed (v_a)	15 m/s
Minimum turn radius in the horizontal plane (r_h)	34.56 m
Minimum turn radius in the vertical plane (r_v)	114.56 m
Maximum load factor (η)	1.2002
Acceleration due to gravity (g)	9.81 m/s^2

Sufficient distance between initial and final points to obtain a CSC path:

It can be observed that CSC path can exist only if there is a common tangent between the initial and final circular turns. Now, if the distance between these two circles are not large enough and the circles touch each other the path will become CC type. Let us consider the geometry of the CC path shown in Figure 5. Form this figure one can write that,

$$\|\boldsymbol{X_0X_f}\| = \|\boldsymbol{OX_f} - \boldsymbol{OX_0}\| = \|(\boldsymbol{OX_f} - \boldsymbol{OP}) + (\boldsymbol{OP} - \boldsymbol{OX_0})\| \quad (25)$$

Using triangular inequality we get,

$$\|\boldsymbol{X_0X_f}\| = \|\boldsymbol{OX_f} - \boldsymbol{OX_0}\| \leq \|(\boldsymbol{OX_f} - \boldsymbol{OP})\| + \|(\boldsymbol{OP} - \boldsymbol{OX_0})\| \quad (26)$$

Where, $\|(\boldsymbol{OX_f} - \boldsymbol{OP})\| \leq 2r_2$ and $\|(\boldsymbol{OP} - \boldsymbol{OX_0})\| \leq 2r_1$.

Again note that, $r_1 \leq r_v$ and $r_2 \leq r_v$

So to ensure that there is a common tangent between these two turns or to ensure that CSC path exists for a given initial and final configurations, one needs to check whether $\|\boldsymbol{X}_0\boldsymbol{X}_f\| > 4r_v$.

4. SIMULATION RESULTS

To show the efficiency of the algorithm a number of configurations are considered for simulation studies as in Table 3. It may be noted that the geometrical distances between initial to final positions are the same for all cases and the value is equal to 707.11 m. The simulation parameters are tabulated in Table 2, which is the same as used in reference[13]. The optimal CSC paths for Case 1 to Case 8 are shown in Figure 6(a) to 6(h), and the path lengths are listed in Table 3.

Table 3: Initial and final configurations for simulation

Case	X_0 (m)	$\boldsymbol{v}_1$	X_f (m)	$\boldsymbol{v}_2$	**Length of CSC path** (m)
Case 1	(0, 0, 0)	(1, 1, 1) / $\sqrt{3}$	(300, 400, 500)	(1, 1, 1) / $\sqrt{3}$	707.41
Case 2	(0, 0, 0)	(1, 1, 1) / $\sqrt{3}$	(-300, 400, 500)	(1, 1, 1) / $\sqrt{3}$	749.48
Case 3	(0, 0, 0)	(1, 1, 1) / $\sqrt{3}$	(-300, -400, 500)	(1, 1, 1) / $\sqrt{3}$	952.27
Case 4	(0, 0, 0)	(1, 1, 1) / $\sqrt{3}$	(300, -400, 500)	(1, 1, 1) / $\sqrt{3}$	778.96
Case 5	(0, 0, 0)	(1, 1, 1) / $\sqrt{3}$	(300, 400, -500)	(1, 0, 0)	795.65
Case 6	(0, 0, 0)	(1, 1, 1) / $\sqrt{3}$	(-300, 400, -500)	(1, 0, 0)	946.75
Case 7	(0, 0, 0)	(1, 1, 1) / $\sqrt{3}$	(-300, -400, -500)	(1, 0, 0)	1075.6
Case 8	(0, 0, 0)	(1, 1, 1) / $\sqrt{3}$	(300, -400, -500)	(1, 0, 0)	873.46

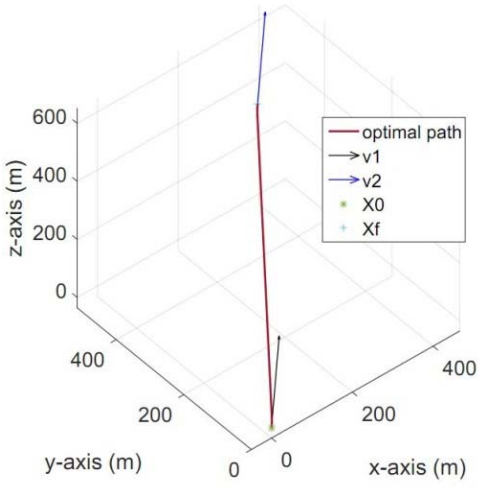

(a) Case 1

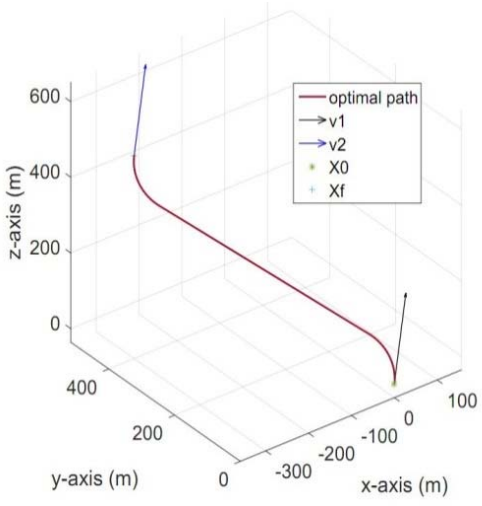

(b) Case 2

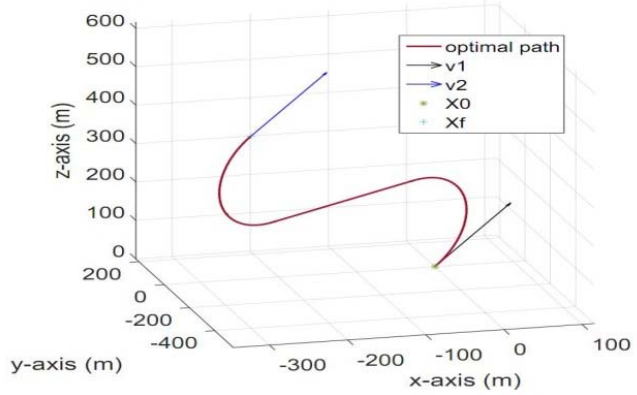

(c) Case 3

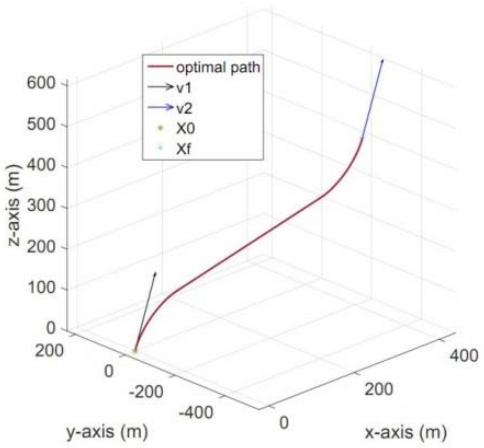

(d) Case 4

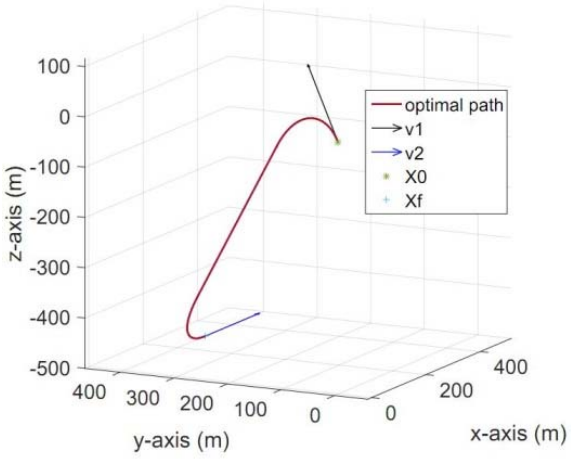

(e) Case 5

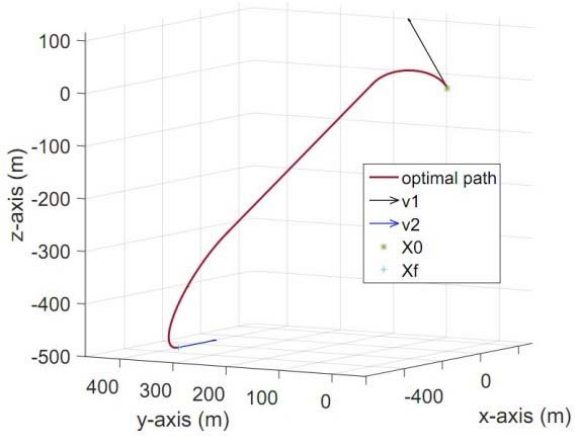

(f) Case 6

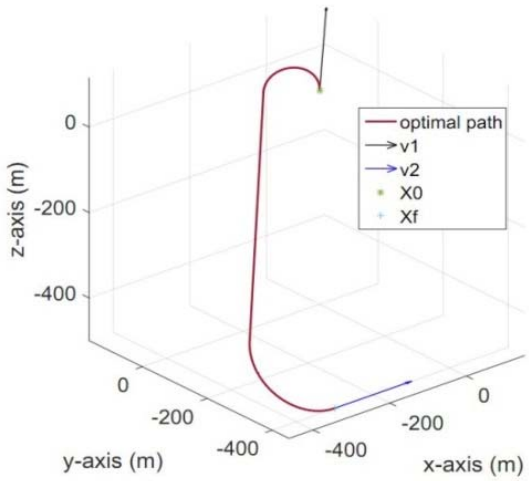

(g) Case 7

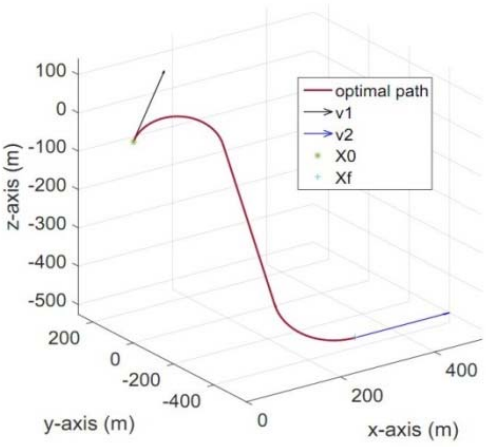

(h) Case 8

Figure 6: Optimal CSC paths in 3D space for Case 1-8.

5. CONCLUSION

The geometrical method has been developed for path planning of an aerial vehicle in 3D space with different values of minimum turn radius in different inclined planes. The method is very effective and fast enough to implement in real-time when the initial and final points are given, and they are situated sufficiently far from each other. Using the method discussed in the present work, four CSC paths can be obtained; one of them is the optimal one. Using this technique waypoint following problems can be solved in minimum time, which can save time as well as the fuel consumption of aerial vehicles for a mission which requires a longer duration of time for its completion. The present work can be extended for 3D waypoint following problems in obstacle- filled environments.

REFERENCES

1. L. E. Dubins, ”On curves of minimal length with a constraint on average curvature, and with prescribed initial and terminal positions and tangents,” *American Journal of Mathematics*, vol. 79, pp. 497-516, 1957.
2. A. M. Shkel, and V. J. Lumelsky, ”Classification of Dubins set,” *Robotics and Autonomous Systems*, vol. 34, pp. 179-202, 2001.
3. M. Shanmugavel, A. Tsourdos, B. A. White, and R. Zbikowski, ”Differential geometric path planning of multiple UAVs,” *Journal of Dynamic Systems, Measurement, and Control*, vol. 129, pp. 620-632, Sep. 2007.
4. A. R. Babaei, and M. Mortazavi, ”Fast trajectory planning based on inflight waypoints for unmanned aerial vehicles,” *Aircraft Engineering and Aerospace Technology*, vol. 82, no. 2, pp. 107-115, 2010.
5. S. Hota, and D. Ghose, ”A modified Dubins method for optimal path planning of a miniature air vehicle converging to a straight line path,” *Proceedings of the American Control Conference, St. Louis, Missouri, USA*, pp. 2397-2402, June 2009.
6. D. R. Nelson, D. B. Barber, T. W. Mclain, and R. W. Beard, ”Vector field path following for miniature air vehicles,” *IEEE Transactions on Robotics*, vol. 23, no. 3, pp. 519-529, June 2007.
7. S. Park, J. Deyst, and J. P. How, ”Performance and Lyapunov stability of a nonlinear path-following guidance method,” *Journal of Guidance, Control, and Dynamics*, vol. 30, no. 6, pp. 1718-1728, Nov. 2007.
8. S. Hota, and D. Ghose, ”Curvature-constrained trajectory generation for waypoint following for miniature aerial vehicles,” *Journal of Aerospace Engineering*, vol. 228, no. 11, pp. 2066-2082, 2014.
9. H. J. Sussmann, ”Shortest 3-dimensional paths with a prescribed curvature bound,” *34th IEEE Conference on Decision and Control, New Orleans*, pp. 3306-3312, 1995.
10. S. Hota, and D. Ghose, ”Optimal path planning for an aerial vehicle in 3D space,” *49th IEEE Conference on Decision and Control (CDC)*, pp. 4902-4907, Dec. 2010.
11. P. Pharpatara, B. Herisse, and Y. Bestaoui, ”3D-shortest paths for a hypersonic glider in a heterogeneous environment,” *IFAC-PapersOnline*, vol. 48, no. 9, pp. 186-191, 2015.
12. H. Cicibas, K. A. Demir, and N. Arica, ”Comparison of 3D versus 4D path planning for unmanned aerial vehicles,” *Defence Science Journal*, vol. 66, no. 6, pp. 651-664, Nov. 2016.
13. S. Hota, and D. Ghose, ”Waypoint-based trajectory planning of fixed-wing MAVs in 3D space,” *Journal of Intelligent & Robotic Systems*, vol. 86, no. 1, pp. 95–113, 2017.
14. P. Pharpatara, B. Herisse, and Y. Bestaoui, ”3-D trajectory planning of aerial vehicles using RRT*,” *IEEE Transactions on Control Systems Technology*, vol. 25, no. 3, pp. 1116-1123, May 2017.